

Resonant x-ray scattering reveals possible disappearance of magnetic order under hydrostatic pressure in the Kitaev candidate γ -Li₂IrO₃

Nicholas P. Breznay,^{1,2,*} Alejandro Ruiz,^{1,2} Alex Frano,^{1,3} Wenli Bi,^{4,5} Robert J. Birgeneau,¹ Daniel Haskel,⁴ and James G. Analytis^{1,2}

¹*Department of Physics, University of California, Berkeley, Berkeley CA 94720, USA*

²*Materials Science Division, Lawrence Berkeley National Laboratory, Berkeley CA 94720, USA*

³*Advanced Light Source, Lawrence Berkeley National Laboratory, Berkeley CA 94720, USA*

⁴*Advanced Photon Source, Argonne National Laboratory, Argonne, Illinois 60439, USA*

⁵*Department of Geology, University of Illinois at Urbana-Champaign, Urbana IL 61801, USA*

(Dated: March 3, 2017)

Honeycomb iridates such as γ -Li₂IrO₃ are argued to realize Kitaev spin-anisotropic magnetic exchange, along with Heisenberg and possibly other couplings. While systems with pure Kitaev interactions are candidates to realize a quantum spin liquid ground state, in γ -Li₂IrO₃ it has been shown that the balance of magnetic interactions leads to the incommensurate spiral spin order at ambient pressure below 38 K. We study the fragility of this state in single crystals of γ -Li₂IrO₃ using resonant x-ray scattering (RXS) under applied hydrostatic pressures of up to 3.0 GPa. RXS is a direct probe of the underlying electronic order, and we observe the abrupt disappearance of the $\mathbf{q}=(0.57, 0, 0)$ spiral order at a critical pressure $P_c = 1.5$ GPa with no accompanying change in the symmetry of the lattice. This dramatic disappearance is in stark contrast with recent studies of β -Li₂IrO₃ that show continuous suppression of the spiral order in magnetic field; under pressure, a new and possibly nonmagnetic ground state emerges.

Introduction-Honeycomb magnetic materials with strong spin-orbit coupling were recently proposed to realize spin-anisotropic “Kitaev” magnetic exchange¹ and therefore to host a highly entangled spin-liquid ground state with fractionalized excitations^{2,3}. Additional interactions (such as Heisenberg or next-nearest-neighbor couplings) that compete with the Kitaev exchange leads to complex landscapes of possible spin orders⁴⁻⁸. For example, the layered compounds Na₂IrO₃ and RuCl₃, composed of edge-sharing IrO₆ or RuCl₆ octahedra, show a “zig-zag” spin texture that onsets below 10-15 K⁹⁻¹¹. The three-dimensional (3D) ‘harmonic’ honeycomb β and γ polytypes of Li₂IrO₃^{12,13} both exhibit an incommensurate spiral order^{14,15}. These magnetic ground states derive from the balance of Kitaev (K), Heisenberg (J), and other possible couplings between spins \vec{S}_i in the Hamiltonian

$$H = \sum_{\substack{i,j \\ \gamma \in x,y,z}} \left(K S_i^\gamma S_j^\gamma + J \vec{S}_i \cdot \vec{S}_j + \dots \right). \quad (1)$$

Here the $\gamma = x, y, z$ Kitaev exchange directions couple spins that are perpendicular to the planes formed by adjacent IrO₆ octahedra, shown for γ -Li₂IrO₃ in Fig. 1AB.

Precisely tuning the relative strength of these magnetic interactions remains an outstanding challenge. Recent resonant x-ray scattering (RXS) studies of β -Li₂IrO₃ indicate that a magnetic field both suppresses the spiral order and stabilizes a canted zig-zag spin texture¹⁶, while magnetic circular dichroism studies of β -Li₂IrO₃ under hydrostatic pressure (and also in applied fields) suggest a disappearance of the magnetic order near 2 GPa. Studies of Sr₂IrO₄ indicate quenching of the ferromagnetic moments at 17 GPa¹⁷ and demonstrate that hydrostatic pressure can be a useful control parameter in these mate-

rials. However, to date there have been no direct probes of the spiral (or other non-ferromagnetic) order under pressure in the honeycomb iridates.

An unambiguous probe of electronic orders resolved in Q -space is RXS. In this technique, the energy of incident x-rays is tuned to be on resonance with an element’s absorption edge and so it is sensitive to both charge and magnetic order of the valence electrons¹⁸. At the Ir $L_{2,3}$ -edge, for example, the intermediate states in the scattering process are sensitive to both the spin and orbital character of the 5d hole states. RXS is particularly useful when neutron scattering is rendered unfeasible by small sample sizes or elements with large neutron absorption cross sections like iridium. Thus, the enhanced cross section at the Ir L_3 -resonance along with the large Ewald sphere afforded by 11.215 keV x-rays have made RXS the best suited scattering technique to investigate the ambient pressure magnetic order in the honeycomb iridates γ -Li₂IrO₃¹⁵, β -Li₂IrO₃¹⁴, and Na₂IrO₃¹⁹. Conducting RXS at the Ir L_3 -edge under applied pressure is possible in reflection and transmission modes²⁰, but both modes are constrained by the geometry of a high pressure apparatus and resulting limitations on the sample geometry and available reciprocal space. Hence magnetic RXS at non-ambient pressures represents an acute experimental challenge.

In this work, we modify the magnetic ground state in the 3D honeycomb iridate γ -Li₂IrO₃ by applying hydrostatic pressure and observe the disappearance of the incommensurate spiral order using RXS. In contrast to recent studies that use symmetry-breaking magnetic fields^{13,16}, here we observe disappearance of the spiral order with no observed discontinuity in the lattice structure to the highest pressures measured. The abrupt disappearance of the spiral Bragg peak at a critical pressure

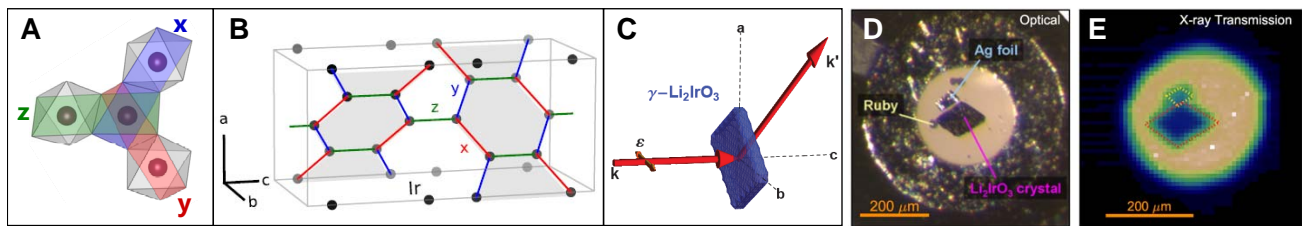


FIG. 1. (A) Local geometry of edge-sharing IrO_6 octahedra, and (B) 3D network of Ir atoms composed of intersecting honeycomb layers (gray) in the orthorhombic crystal structure of $\gamma\text{-Li}_2\text{IrO}_3$; x , y , z Kitaev bonds are highlighted in both panels. (C) Laue (transmission) scattering geometry; x-rays with initial wavevector \mathbf{k} and polarization ϵ scatter into \mathbf{k}' within the Li_2IrO_3 crystallographic a - c plane. (D) Micrograph of the loaded diamond anvil cell with polished single crystal, and Ag foil and ruby spheres for pressure calibration and *in-situ* monitoring. (E) X-ray transmission image of the sample *in-situ*; both $\gamma\text{-Li}_2\text{IrO}_3$ crystal and Ag foil are outlined.

$P_c = 1.5$ GPa signals the transition to a distinct electronic ground state.

Experimental—We track the disappearance of the spiral magnetic order in $\gamma\text{-Li}_2\text{IrO}_3$ using RXS on oriented single crystal samples. The transmission scattering scheme, shown in Fig. 1C, allows access to the $(H\ 0\ 0)$ direction in specular diffraction using horizontally (σ) polarized photons in a vertical geometry and with no polarization analysis of the scattered beam. The magnetic scattering intensity, proportional to $|\sum_i e^{i\mathbf{Q}\cdot\mathbf{r}_i} (\boldsymbol{\sigma} \times \boldsymbol{\pi}_{out}) \cdot \mathbf{m}_i|^{218}$, where \mathbf{m}_i is the magnetic moment at site r_i , projects out the component of \mathbf{m}_i parallel to \mathbf{k}' (in the a - c scattering plane).

Crystals of $\gamma\text{-Li}_2\text{IrO}_3$ were grown as described previously^{12,16}. Figure 1B shows the intersecting Ir honeycomb layers in one unit cell of the orthorhombic C_{ccm} crystal structure. For the transmission (Laue) scattering geometry, we polished single crystals to 20-30 μm thick; the absorption length of x-rays near the Ir $L_{2,3}$ edges is ≈ 10 μm .

X-ray scattering studies under pressure (up to 5 GPa) and at temperatures between 5-300 K were performed at beamline 4-ID-D of the Advanced Photon Source at Argonne National Lab. Merrill-Bassett type diamond anvil cells (DAC) with 800 μm culets were used with stainless steel gaskets of 250 (150) μm initial (pre-indented) thicknesses, with 400 μm sample chamber holes²¹. The gaskets were loaded with $\gamma\text{-Li}_2\text{IrO}_3$ single crystals (cross-sectional area 150×100 μm^2 , polished thickness 25 μm), along with several ruby balls and 40×40 μm^2 pieces of 12 μm thick Ag foil for ambient- and low-temperature pressure calibration²². The pressure medium was a 4:1 methanol:ethanol mixture. After initial loading, the pressure at ambient temperature was monitored using a custom-built optical spectrometer and a Raman system to measure the ruby $R1$ fluorescence peak; the target pressure upon loading was ~ 0.1 GPa. The pressure at low temperature was determined in situ using Ag powder peaks and the isothermal bulk modulus of Ag at 5 K ($K_{\text{Ag}} = 110.85$ GPa, $K'_{\text{Ag}} = 6.0$ GPa)²². We estimate a systematic uncertainty of ± 0.1 GPa in the pressures quoted below by comparing the estimated pressure from $(1\ 1\ 1)$,

$(2\ 0\ 0)$, and $(2\ 2\ 0)$ Ag powder peaks, and from repeated pressure measurements before and after scans.

Two samples were cooled, aligned in the diffractometer, and studied; all measurements reported here were performed at the cryostat base temperature of 4.5 ± 0.5 K. Pressure was changed *in situ* using a helium membrane. Cell layout and sample status were checked after loading (see optical image in Fig. 1D, showing diamond-shaped $\gamma\text{-Li}_2\text{IrO}_3$ crystal, Ag foil, and ruby spheres in the DAC gasket hole) and monitored in-situ using both x-ray transmission maps (Fig. 1E, obtained using a slit-defined 30×30 μm^2 beam). To track the absolute magnetic Bragg peak intensities with pressure, peak areas were normalized to the integrated $(4\ 0\ 0)$ rocking curve intensities. The mosaic full-width at half-maximum is 0.05 - 0.10° for sample 1 between 0-3 GPa, and 0.01° for sample 2 at 2.0 GPa.

Results—Based on the restricted scattering geometry imposed by the DAC, we focused our study on $(H\ 0\ 0)$ peaks in reciprocal space. In $\gamma\text{-Li}_2\text{IrO}_3$, selection rules forbid the $(1\ 0\ 0)$ and $(3\ 0\ 0)$ lattice peaks, while the structure factor for the $(2\ 0\ 0)$ order is strongly suppressed. Figure 2A shows a reciprocal space map of the $(H\ 0\ 0)$ axis, where an intense structural $(4\ 0\ 0)$ Bragg peak and weaker $(2\ 0\ 0)$ peak are both observed. (In the $\beta\text{-Li}_2\text{IrO}_3$ polytype the $(2\ 0\ 0)$ peak is forbidden.) Non-structural peaks located at $(4 \pm 0.57\ 0\ 0)$ correspond to the incommensurate spiral magnetic order^{14,15}, which at ambient pressure onsets at $T_{\text{sp}} = 38$ K. The electronic nature of these peaks is confirmed by fixed- Q energy scans (Fig. 2C) showing a strong enhancement of the diffracted intensity near the 11.215 keV Ir L_3 resonance, in contrast to the weak background observed away from the spiral order peak at $(3.85\ 0\ 0) + \mathbf{q}$ that shows an increase of $\sim 10\%$ above the Ir edge due to fluorescence.

Figure 3 shows the pressure dependence of the $(4\ 0\ 0)$ Bragg peak (normalized), as well as the spiral order peak. Note that the shift in the 3.3 GPa $(4\ 0\ 0)$ scan is a consequence of a large pressure increment; the a -axis lattice parameter evolves linearly with pressure over the entire range studied. Neither the $(4\ 0\ 0)$ Bragg peak nor \mathbf{q} peak widths change appreciably with increasing

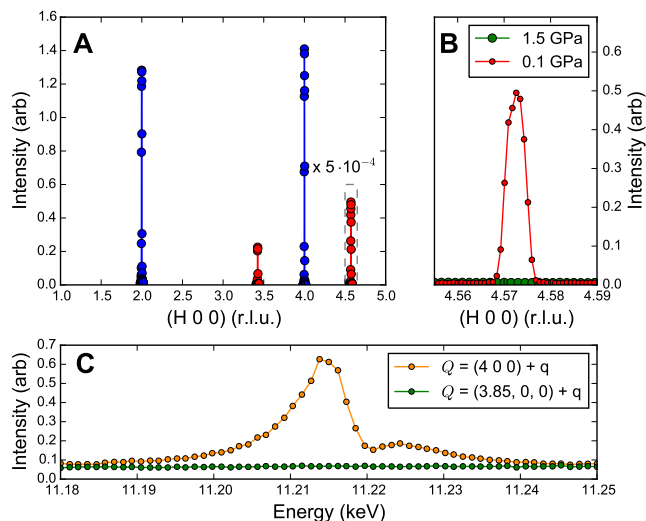


FIG. 2. (A) Magnetic (red) and structural (blue) Bragg peaks along the $(H\ 0\ 0)$ direction measured at 4.5 K; the $(4\ 0\ 0)$ peak has been scaled by a factor of 5×10^{-4} . (B) Zoom-in of the dashed region in (A) showing scans near $(4\ 0\ 0) + \mathbf{q} = (4.57\ 0\ 0)$. The magnetic Bragg peak visible at 0.1 GPa (red) disappears abruptly above 1.5 GPa (green). (C) Energy scans at fixed $\mathbf{Q} = (4.57\ 0\ 0)$ (orange) and away from the magnetic peak $\mathbf{Q} = (4.42\ 0\ 0)$ showing a featureless background.

pressure, indicating that both the crystal quality and long range nature of the spiral order remain constant. Figure 4D shows the evolution of the a -axis lattice parameter with pressure, along with a linear fit yielding $da/dP = -0.015 \text{ \AA}/\text{GPa}$. Assuming an isotropic fractional change in the unit cell dimensions, the $T = 4.5\ \text{K}$ bulk modulus $K = -\frac{1}{3} a \left(\frac{da}{dP} \right)^{-1} = 130 \pm 20\ \text{GPa}$. Recent electronic structure calculations for $\beta\text{-Li}_2\text{IrO}_3$ indicate an anisotropic compressibility²³ with a more compressible than c ; this would increase K relative to the above estimate and be quite comparable to the 150-250 GPa observed in Sr_2IrO_4 and $\text{Sr}_3\text{Ir}_2\text{O}_7$ compounds^{20,24}, and recent studies of $\beta\text{-Li}_2\text{IrO}_3$ powders²⁵.

Under an applied pressure of $P_c = 1.5\ \text{GPa}$, the spiral order peaks are abruptly extinguished as shown in Fig. 2B for peaks at $(4\ 0\ 0) + \mathbf{q}$. We scanned the entire accessible range of $2 < H < 6$ r.l.u. and found no evidence for the incommensurate peaks anywhere in this region. Aside from contraction of the unit cell (shown in Fig. 4D), no structural changes were observed; the symmetry of the lattice appears intact throughout this pressure range. Figure 4A shows the integrated peak intensity for \mathbf{q} as a function of applied pressure, measured at 4.5 K incrementally beginning at 0.5 GPa. To within the uncertainty associated with consistent re-alignment of the sample after changing pressure, the peak intensities gradually increase with pressure until abruptly disappearing at P_c . An (otherwise identical) additional sample also showed no sign of the spiral order at the after-cool-down pressure of 2.0 GPa. The incommensurate wavevec-

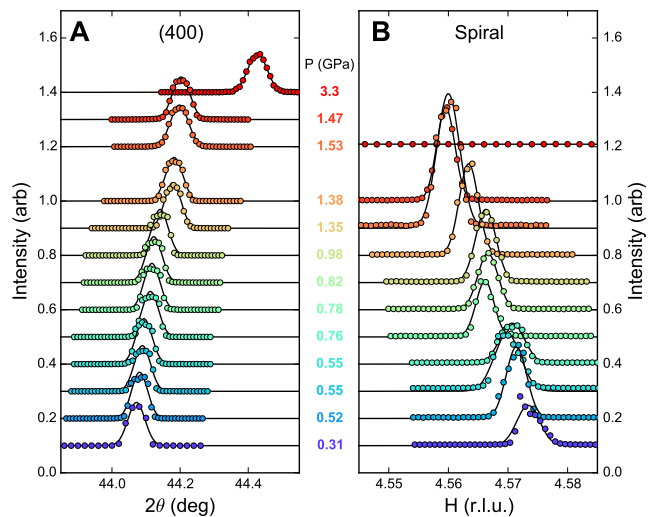


FIG. 3. (A) (400) Bragg peak intensity versus 2θ and (B) evolution of spiral order $(4.57\ 0\ 0)$ peaks with applied pressures from 0.3 to 3.0 GPa as labeled for both plots. Solid lines are guides to the eye.

tor \mathbf{q} , normalized to the change in lattice constant, decreases with increasing pressure as shown in Fig. 4B; \mathbf{q} decreases by 0.3% before the spiral order disappears at P_c . The linear and continuous decrease observed in \mathbf{q} , ending at an apparently irrational fraction, precludes an incommensurate-to-commensurate transition.

Discussion—Figure 4C presents a schematic pressure-temperature phase diagram for $\gamma\text{-Li}_2\text{IrO}_3$. Ongoing studies of this material indicate paramagnetic behavior with rapidly emerging magnetic anisotropy favoring the b (easy) axis direction^{12,26} at ambient pressure. With increasing pressure and as $T \rightarrow 0$, P_c likely continues to represent a sharp phase boundary between the spiral magnetic order and the as-yet undetermined high-pressure electronic phase. As there is no change in the lattice symmetry, and no symmetry-breaking field being used to perturb the material, it is unclear what ordered state may exist beyond P_c , if any. Under an applied magnetic field, a canted zig-zag order appears to be the next competitive magnetic ground state at ambient pressure¹⁶. However the transition observed under applied fields appears to be continuous, in contrast to the transition at P_c , indicating that a different ground state emerges in this case.

The effect of pressure on the crystal structure and associated Kitaev, Heisenberg, and other exchange couplings, was recently studied theoretically for $\beta\text{-Li}_2\text{IrO}_3$ ²³. In this closely related polytype, the Kitaev exchange coupling was predicted to decrease with increasing pressure above ambient, disappearing at 5-10 GPa. If similar evolution of the magnetic interactions appears in $\gamma\text{-Li}_2\text{IrO}_3$, our results strongly suggest that the spiral magnetic order is stabilized by Kitaev exchange and suppressed as this mechanism weakens. Precise experimental description of structural distortion with increasing pressure in

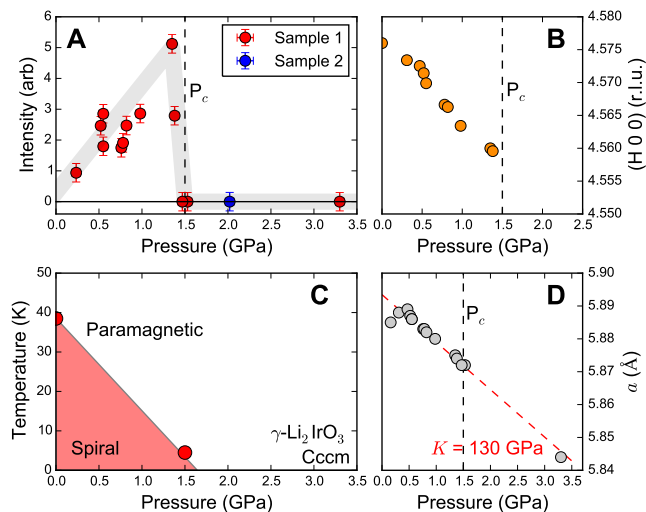


FIG. 4. (A) Magnetic Bragg peak intensity versus applied pressure for two samples; the intensity for sample 1 disappears abruptly at $P_c=1.5$ GPa; no magnetic is observed at 2.0 GPa for sample 2. (B) Decrease in the spiral order wavevector $\mathbf{Q}=(H 0 0)$ with applied pressure; the wavevector is not close to a commensurate value at P_c . (C) Pressure-temperature magnetic phase diagram for γ -Li₂IrO₃; no discontinuous change in the lattice is observed to 3.0 GPa. (D) Decrease in a with applied hydrostatic pressure, extracted from the (4 0 0) structural Bragg peak; assuming a relative change in volume that is isotropic, the bulk modulus $K = 130$ GPa.

both Li₂IrO₃ polytypes will allow for a quantitative analysis of how the change in structure serves to push this material closer to or farther from the pure Kitaev limit.

The scale of P_c is modest compared to the 17 GPa required to suppress weak ferromagnetism in Sr₂IrO₄¹⁷. The pressure roughly corresponds to an energy density of 9 meV/Å³, or 0.08 eV/Ir; while less than both the spin-orbital energy $\lambda_{SO} \sim 0.2 - 0.5$ eV as well as electronic interaction $U \sim 0.5$ eV that have been reported in 5d iridate materials^{17,27,28}, it is beyond the ~ 1 meV scale

that was proposed to separate β -Li₂IrO₃ from a 3D spin liquid state²⁹. Mixing of the (nominally filled) $J = 3/2$ manifold of states could serve to disrupt the $J_{\text{eff}} = 1/2$ doublet that is crucial to the stability of unconventional magnetic orders in these materials. Such a picture could be investigated quantitatively with high-pressure studies of x-ray absorption (XAS) and magnetic circular dichroism (XMCD) spectroscopies that provide a quantitative probe of the spin and orbital components of the local magnetic moments.

Summary—By conducting resonant x-ray scattering studies at the Ir L_3 edge, we are able to observe the disappearance of the spiral magnetic order in γ -Li₂IrO₃ at an applied pressure of 1.5 GPa. This observation provides strong evidence for tunability of the Kitaev, Heisenberg, and other magnetic exchange couplings with applied pressure. Future resonant diffraction studies will be able to incisively address the possibility of complete disappearance of long range magnetic order in the high pressure ground state of this Kitaev candidate material.

ACKNOWLEDGMENTS

The authors thank Z. Islam, Y. Choi, and the support staff at APS Sector 4 for their assistance, and P. Moll and J. Reuteler at Scope-M ETH for additional sample preparation. This work was supported by the U.S. Department of Energy, Office of Science, Basic Energy Sciences under Award No. DE-SC0014039. This research used resources of the Advanced Photon Source, a U.S. Department of Energy (DOE) Office of Science User Facility operated for the DOE Office of Science by Argonne National Laboratory under Contract No. DE-AC02-06CH11357. NPB was supported by the Gordon and Betty Moore Foundations EPIQS Initiative through Grant GBMF4374. AF acknowledges support from the University of California Presidents Postdoctoral Fellowship Program. WB acknowledges partial support from COMPRES, the Consortium for Materials Properties Research in Earth Sciences under NSF Cooperative Agreement EAR 1606856.

* nbreznay@berkeley.edu

¹ G. Jackeli and G. Khaliullin. Mott insulators in the strong spin-orbit coupling limit: From heisenberg to a quantum compass and kitaev models. *Physical Review Letters*, 102(1):017205, January 2009.

² A Kitaev. Anyons in an exactly solved model and beyond. *Annals of Physics*, 321(1):2–111, January 2006.

³ William Witczak-Krempa, Gang Chen, Yong Baek Kim, and Leon Balents. Correlated quantum phenomena in the strong spin-orbit regime. *Annual Review of Condensed Matter Physics*, 5(1):57–82, 2014.

⁴ Jiri Chaloupka, George Jackeli, and Giniyat Khaliullin. Kitaev-heisenberg model on a honeycomb lattice: Possible exotic phases in iridium oxides a₂iro₃. *Phys. Rev. Lett.*,

105:027204, Jul 2010.

⁵ Yogesh Singh, S. Manni, J. Reuther, T. Berlijn, R. Thomale, W. Ku, S. Trebst, and P. Gegenwart. Relevance of the heisenberg-kitaev model for the honeycomb lattice iridates a₂IrO₃. *Physical Review Letters*, 108(12):127203, March 2012.

⁶ Eric Kin-Ho Lee and Yong Baek Kim. Theory of magnetic phase diagrams in hyperhoneycomb and harmonic-honeycomb iridates. *Phys. Rev. B*, 91:064407, Feb 2015.

⁷ Itamar Kimchi, Radu Coldea, and Ashvin Vishwanath. Unified theory of spiral magnetism in the harmonic-honeycomb iridates α, β , and γ Li₂iro₃. *Phys. Rev. B*, 91:245134, Jun 2015.

⁸ Stephen M. Winter, Ying Li, Harald O. Jeschke, and Roser

- Valentí. Challenges in design of kitaev materials: Magnetic interactions from competing energy scales. *Phys. Rev. B*, 93:214431, Jun 2016.
- ⁹ Ji? Chaloupka, George Jackeli, and Giniyat Khaliullin. Zigzag magnetic order in the iridium oxide Na_2IrO_3 . *Physical Review Letters*, 110(9):097204, February 2013.
- ¹⁰ R. D. Johnson, S. C. Williams, A. A. Haghhighirad, J. Singleton, V. Zapf, P. Manuel, I. I. Mazin, Y. Li, H. O. Jeschke, R. Valentí, and R. Coldea. Monoclinic crystal structure of $\alpha\text{-RuCl}_3$ and the zigzag antiferromagnetic ground state. *Phys. Rev. B*, 92:235119, Dec 2015.
- ¹¹ J. A. Sears, M. Songvilay, K. W. Plumb, J. P. Clancy, Y. Qiu, Y. Zhao, D. Parshall, and Young-June Kim. Magnetic order in $\alpha\text{-RuCl}_3$: A honeycomb-lattice quantum magnet with strong spin-orbit coupling. *Phys. Rev. B*, 91:144420, Apr 2015.
- ¹² K. A. Modic, Tess E. Smidt, Itamar Kimchi, Nicholas P. Breznay, Alun Biffin, Sungkyun Choi, Roger D. Johnson, Radu Coldea, Pilanda Watkins-Curry, Gregory T. McCandless, Julia Y. Chan, Felipe Gandara, Z. Islam, Ashvin Vishwanath, Arkady Shekhter, Ross D. McDonald, and James G. Analytis. Realization of a three-dimensional spin-anisotropic harmonic honeycomb iridate. *Nature Communications*, 5, jun 2014.
- ¹³ T. Takayama, A. Kato, R. Dinnebier, J. Nuss, H. Kono, L. S. I. Veiga, G. Fabbris, D. Haskel, and H. Takagi. Hyperhoneycomb iridate $\beta\text{-Li}_2\text{IrO}_3$ as a platform for kitaev magnetism. *Phys. Rev. Lett.*, 114:077202, Feb 2015.
- ¹⁴ A. Biffin, R. D. Johnson, Sungkyun Choi, F. Freund, S. Manni, A. Bombardi, P. Manuel, P. Gegenwart, and R. Coldea. Unconventional magnetic order on the hyperhoneycomb Kitaev lattice in $\beta\text{-Li}_2\text{IrO}_3$: Full solution via magnetic resonant x-ray diffraction. *Physical Review B*, 90(20):205116, nov 2014.
- ¹⁵ A. Biffin, R.D. Johnson, I. Kimchi, R. Morris, A. Bombardi, J.G. Analytis, A. Vishwanath, and R. Coldea. Noncoplanar and Counterrotating Incommensurate Magnetic Order Stabilized by Kitaev Interactions in $\gamma\text{-Li}_2\text{IrO}_3$. *Physical Review Letters*, 113(19):197201, November 2014.
- ¹⁶ A. Ruiz, A. Frano, N. P. Breznay, Z. Islam, T. Helm, I. Oswald, J. Y. Chan, and J. G. Analytis. (*unpublished*), 2016.
- ¹⁷ D. Haskel, G. Fabbris, Mikhail Zhernenkov, P. P. Kong, C. Q. Jin, G. Cao, and M. van Veenendaal. Pressure tuning of the spin-orbit coupled ground state in Sr_2IrO_4 . *Phys. Rev. Lett.*, 109:027204, Jul 2012.
- ¹⁸ J. P. Hannon, G. T. Trammell, M. Blume, and Doon Gibbs. X-ray resonance exchange scattering. *Phys. Rev. Lett.*, 61:1245–1248, Sep 1988.
- ¹⁹ X. Liu, T. Berlijn, W.-G. Yin, W. Ku, A. Tsvelik, Young-June Kim, H. Gretarsson, Yogesh Singh, P. Gegenwart, and J. P. Hill. Long-range magnetic ordering in Na_2IrO_3 . *Phys. Rev. B*, 83:220403, 2011.
- ²⁰ D. Haskel, G. Fabbris, J. W. Kim, J. H. Kim, B. Kim, G. Cao, V. Struzhkin, P. P. Stavropoulos, H-S. Kim, H-Y. Kee, and S. Todadri. (*unpublished*).
- ²¹ Yejun Feng, R. Jaramillo, Jiyang Wang, Yang Ren, and T. F. Rosenbaum. Invited article: High-pressure techniques for condensed matter physics at low temperature. *Review of Scientific Instruments*, 81(4):041301, 2010.
- ²² W. B. Holzapfel, M. Hartwig, and W. Sievers. Equations of state for Cu, Ag, and Au for wide ranges in temperature and pressure up to 500 GPa and above. *Journal of Physical and Chemical Reference Data*, 30(2):515–529, 2001.
- ²³ Heung-Sik Kim, Yong Baek Kim, and Hae-Young Kee. Revealing frustrated local moment model for pressurized hyperhoneycomb iridate: Paving the way toward a quantum spin liquid. *Phys. Rev. B*, 94:245127, Dec 2016.
- ²⁴ Z. Zhao, S. Wang, T. F. Qi, Q. Zeng, S. Hirai, P. P. Kong, L. Li, C. Park, S. J. Yuan, C. Q. Jin, G. Cao, and W. L. Mao. Pressure induced second-order structural transition in $\text{Sr}_3\text{Ir}_2\text{O}_7$. *Journal of Physics: Condensed Matter*, 26(21):215402, 2014.
- ²⁵ L. S. I. Veiga, M. Etter, K. Glaziryn, F. Sun, G. Fabbris, J. R. L. Mardegan, P. S. Malavi, Y. Deng, M. van Veenendaal, W. G. Yang, J. S. Schilling, T. Takayama, H. Takagi, and D. Haskel. (*unpublished*).
- ²⁶ A. Ruiz, N. P. Breznay, T. Helm, I. Oswald, J. Y. Chan, and J. G. Analytis. (*unpublished*), 2017.
- ²⁷ M. A. Laguna-Marco, D. Haskel, N. Souza-Neto, J. C. Lang, V. V. Krishnamurthy, S. Chikara, G. Cao, and M. van Veenendaal. Orbital magnetism and spin-orbit effects in the electronic structure of BaIrO_3 . *Phys. Rev. Lett.*, 105:216407, Nov 2010.
- ²⁸ J. P. Clancy, N. Chen, C. Y. Kim, W. F. Chen, K. W. Plumb, B. C. Jeon, T. W. Noh, and Young-June Kim. Spin-orbit coupling in iridium-based $5d$ compounds probed by x-ray absorption spectroscopy. *Phys. Rev. B*, 86:195131, Nov 2012.
- ²⁹ Vamshi M. Katukuri, Ravi Yadav, Liviu Hozoi, Satoshi Nishimoto, and Jeroen van den Brink. The vicinity of hyper-honeycomb $\text{-Li}_2\text{IrO}_3$ to a three-dimensional kitaev spin liquid state. *Scientific Reports*, 6:29585, 2016.